Astronomy & Astrophysics manuscript no. paper˙harpsm˙calv˙valt
February 11, 2014

Metallicity of M dwarfs

IV. A high-precision [Fe/H] and T_{eff} calibration in the optical for M dwarfs *

V. Neves[1,2,3], X. Bonfils[2], N. C. Santos[1,3], X. Delfosse[2], T. Forveille[2], F. Allard[4], and S. Udry[5]

[1] Centro de Astrofísica, Universidade do Porto, Rua das Estrelas, 4150-762 Porto, Portugal
email: vasco.neves@astro.ua.pt
[2] UJF-Grenoble 1 / CNRS-INSU, Institut de Planétologie et d'Astrophysique de Grenoble (IPAG) UMR 5274, Grenoble, F-38041, France.
[3] Departamento de Física e Astronomia, Faculdade de Ciências, Universidade do Porto, Rua do Campo Alegre, 4169-007 Porto, Portugal
[4] Centre de Recherche Astrophysique de Lyon, UMR 5574: CNRS, Université de Lyon, École Normale Supérieure de Lyon, 46 Allée d'Italie, F-69364 Lyon Cedex 07, France
[5] Observatoire de Genève, Université de Genève, 51 Chemin des Maillettes, 1290 Sauverny, Switzerland

Received XXX; accepted XXX

ABSTRACT

Aims. In this work we develop a technique to obtain high precision determinations of metallicity and effective temperature of M dwarfs in the optical.
Methods. A new method is presented that makes use of the information of most lines in the 550-690 nm spectral region. It consists in the measurement of pseudo equivalent widths and their correlation with established scales of [Fe/H] and T_{eff}.
Results. Our calibration achieves a *rms* of 0.07 for [Fe/H], 100 K for T_{eff}, and is valid in the (-0.90, 0.25 dex), (2600, 3800 K), and (M0, M5.5) intervals for [Fe/H], T_{eff} and spectral type respectively. We also calculated the $RMSE_V$ which estimates uncertainties of the order of 0.08 dex for the metallicity and of 300 K for the effective temperature. Our calibration is available online at http://www.astro.up.pt/resources/mcal.

Key words. stars: fundamental parameters – stars: late type – stars: low mass – stars: atmospheres – stars: planetary systems

1. Introduction

The precise derivation of M dwarf atmospheric parameters is still very challenging today. Cooler and intrinsically fainter, M dwarfs are not easy to study. As the M subtype increases more molecules form in its atmosphere, making the spectral continuum very hard or impossible to identify, at least in the visible region of the spectrum. Therefore, methods such as atomic line analysis that are dependent on the knowledge of the continuum are suited only for the metal poor and earliest types of M dwarfs (e.g. Woolf & Wallerstein 2005, 2006). On the other hand, spectral synthesis techniques do not reach yet a high precision comparable to FGK dwarf methods, due to the fundamental lack of knowledge of billions of molecular line strengths and transitions, and most studies have reached modest results (e.g. Valenti et al. 1998; Bean et al. 2006). Despite that, some important progress have been made using spectral synthesis fitting to high-resolution spectra in the infrared (Önehag et al. 2012), where the depression of the continuum in some regions is less intense than in the visible region of the spectrum (e.g. Rajpurohit et al. 2013b). However, only a few stars have been measured this way, and the technique lacks external confirmation.

In this context, most parameter determinations, especially metallicity and effective temperature are instead based on calibrations using colours (e.g. Bonfils et al. 2005; Johnson & Apps 2009; Schlaufman & Laughlin 2010; Johnson et al. 2012; Neves et al. 2012) or spectroscopic indexes (e.g. Rojas-Ayala et al. 2010, 2012; Mann et al. 2013a,b; Newton 2013).

Regarding metallicity, some progress has been made in the last few years. A steady improvement was achieved, bringing the typical uncertainties of ± 0.20 dex of the photometric calibrations, below ∼ 0.10 dex in the most recent low-resolution spectroscopic scales in the infrared (e.g. Rojas-Ayala et al. 2012; Mann et al. 2013a; Newton 2013), following the pioneering work of Rojas-Ayala et al. (2010). However a true high-precision determination with a rms of the order of 0.05 dex, on par with the ones obtained for FGK dwarfs (e.g. Santos et al. 2004; Sousa et al. 2007) has not yet been reached **see introduction in Neves et al. (2012).**

For temperature, on the other hand, important uncertainties and systematics still persist today. Although internal precisions are reported to be lower than 100K (e.g. Casagrande et al. 2008; Rojas-Ayala et al. 2012; Boyajian et al. 2012), their suffer from systematics ranging from 150 to 300 K making the determination of accurate temperature for M dwarfs a priority. Boyajian et al. (2012) also presented a new method, based on high precision interferometric measurements of M dwarf radii and bolometric fluxes, that in principle allow a very precise measurement of the effective temperature. However, some doubts still arise regarding the accuracy of the determination of the total

* Based on observations made with the HARPS instrument on the ESO 3.6-m telescope at La Silla Observatory under programme ID 072.C-0488(E)

flux of the stars, based on templates from Pickles (1998), as recently pointed out by Mann et al. (2013b). They have, in turn, also recently presented their own effective temperature method that is very similar to the one of Boyajian et al. (2012) but rely on a combination of their low resolution spectra with BT-SETTL synthetic spectra from Allard et al. (2011) to calculate the bolometric flux. From these high-precision effective temperatures they established four visual and infrared spectroscopic indices, with precisions (but not accuracies) between 62 and 100 K. The latest effort on a T_{eff} scale of M come from Rajpurohit et al. (2013a), where they compare synthetic spectra from the latest BT-SETTL models (Allard et al. 2012) to low-resolution optical spectra. They obtain a better agreement between synthetic and observed spectra when compared with previous models, estimating uncertainties of T_{eff} of the order of 100 K.

In this work we present a new method to try to overcome the aforementioned hurdles and improve on the precision of both metallicity and effective temperature of M dwarfs. This new calibration was briefly presented in the Appendix of Neves et al. (2013) and used to calculate the planet-metallicity relation of the HARPS GTO M dwarf sample (Bonfils et al. 2013). In Sect. 2 we describe in detail our calibration, as well as the sample selection, uncertainty estimation and a test of the calibration as a function of resolution and signal-to-noise ratio (SNR). Afterwards, in Sect. 3, we compare our results with other determinations from the literature. Finally, in Sect 4 we discuss our results.

2. The calibration

Our new calibration is based on the measurement of pseudo equivalent widths (EWs) of most lines/features in the red part of spectra from a sub-sample of the HARPS GTO M dwarf sample (Bonfils et al. 2013). The features are regions of the spectra that are formed by more than one line.The EWs are then correlated with the reference photometric [Fe/H] and T_{eff} scales from Neves et al. (2012) and Casagrande et al. (2008) respectively. This method achieves an increase in precision of both parameters whereas its accuracy is tied to the original calibrations. The methodology is detailed in Sect. 2.1.

The reference [Fe/H] was calculated using stellar parallaxes, V, and K_S magnitudes following the procedure described in Neves et al. (2012). The reference T_{eff} is the average value of the $V-J$, $V-H$, and $V-K$ photometric scales taken from Casagrande et al. (2008). Table 1 lists the quantities used to calculate these parameters. Column 1 shows the star name, column 2 and 3 the right ascension and declination respectively, column 4 the parallax of each star and its associated error, and column 5 the source of the parallax measurement. Column 6 depicts the stellar type of the star, and columns 7 to 10 the V, J, H, and K_S photometry. Lastly, column 11 details the source of the photometry. The spectral type was calculated following the $V-J$ color relation of Lépine et al. (2013) and has a ±0.5 spectral type uncertainty.

2.1. Method

From the 102 stars of the HARPS M-dwarf sample we first selected 61 stars with spectra having a signal to noise higher than 100. For each star we calculated the median of available individual median normalised spectra. The SNR of the individual spectra were added in quadrature.Then, we measured pseudo EWs of lines and features (blended lines) from the spectra in the region between 530 and 690nm, but excluded the features from the region between 686 and 690 nm due to the heavy presence of telluric lines. We define the pseudo equivalent widths as

$$W = \sum \frac{F_{pp} - F_{\lambda}}{F_{pp}} \Delta\lambda, \quad (1)$$

where F_{pp} is the value of the flux between the peaks of the line/feature at each integration step and F_{λ} the flux of the line/feature. The measurements of the EWs are illustrated in Fig. 1, where the 'peak-to-peak' flux corresponds to the red dotted lines and the flux of the star is shown as a black line.

The very high S/N spectrum of the star Gl205 was used as a reference to establish the line/feature regions that were going to be measured in all spectra. We rejected all lines/features with a EW lower than 8 mÅ to ensure that all lines in stars with lower [Fe/H] or/and T_{eff} can be properly measured. Lines with steep slopes are usually joined with adjacent lines, and measured as one feature. At the end of the line selection we obtained 4142 lines/features. An automatic search of the maximum values of ±0.02Å at the extremes of each line/feature is made to make sure that the 'peak-to-peak regions of all lines/features the spectra are effectively covered.

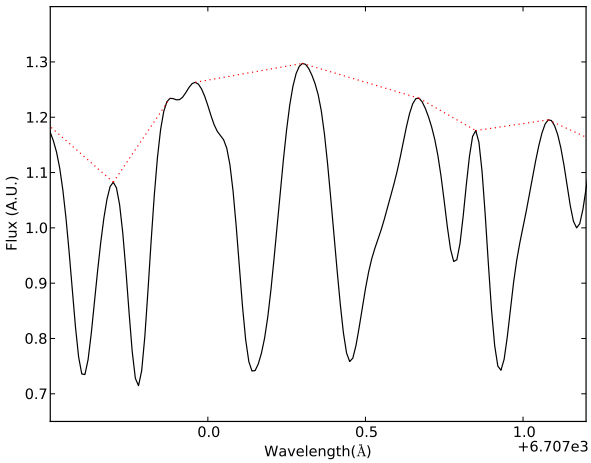

Fig. 1. Small region of the Gl 205 spectra illustrating pseudo equivalent width line measurement. The red dotted line represents the 'peak-to-peak' flux.

The next step consisted in the investigation of the correlation between the measured EWs and the reference values for [Fe/H] and T_{eff}. Fig. 2 shows the histograms of the partial correlation coefficient values of the EWs with the value of the metallicity and effective temperature (solid blue and dashed green lines respectively). The partial correlation coefficient is defined as the correlation coefficient of one parameter keeping the other fixed. We observe, in Fig. 2 that a significant amount of lines have good correlation values with the parameters.

At this stage, we discarded three stars (Gl388, Gl729, Gl803) that were showing bad correlations with either or both the reference metallicity and effective temperature. The cause for the bad correlation is probably due to high activity/rotation. Indeed, the three stars are shown as active in Bonfils et al. (2013). This effect is especially visible in the effective temperature of these stars, where its value is much lower than the reference temperature. For Gl388 and Gl729 Reiners et al. (2012) show that these

Table 1. List containing our sample and the quantities used to calculate the reference [Fe/H] and T_{eff} . Sorted by right ascension.

star	α(2000)	δ(2000)	π [mas]	π source	Spec. Type	V [mag]	J [mag]	H [mag]	K [mag]	V/J/H/K source
Gl1	00:05:25	-37:21:23	230.4 ± 0.9	H	M1.5	8.6 ± 0.02	5.34 ± 0.02	4.73 ± 0.02	4.54 ± 0.02	1/9/9/9
Gl54.1	01:12:31	-17:00:00	271.0 ± 8.4	H	M4.0	12.1 ± 0.02	7.26 ± 0.02	6.75 ± 0.03	6.42 ± 0.02	1/7/7/7
Gl87	02:12:21	+03:34:30	96.0 ± 1.7	H	M1.5	10.0 ± 0.02	6.83 ± 0.02	6.32 ± 0.03	6.08 ± 0.02	1/7/7/7
Gl105B	02:36:16	+06:52:12	139.3 ± 0.5	H	M3.5	11.7 ± 0.02	7.33 ± 0.02	6.79 ± 0.04	6.57 ± 0.02	4/7/7/7
LP771-95A	03:01:51	-16:35:36	146.4 ± 2.9	H06	M2.0	10.6 ± 0.05	7.11 ± 0.02	6.56 ± 0.02	6.29 ± 0.02	2/7/7/7
Gl176	04:42:56	+18:57:29	106.2 ± 2.5	H	M2.0	10.0 ± 0.02	6.46 ± 0.02	5.82 ± 0.03	5.61 ± 0.03	1/7/7/7
Gl191	05:11:40	-45:01:06	255.3 ± 0.9	H	M0.5	8.9 ± 0.02	5.82 ± 0.03	5.32 ± 0.03	5.05 ± 0.02	1/7/7/7
Gl205	05:31:27	-03:40:42	176.8 ± 1.2	H	M1.5	8.0 ± 0.02	4.75 ± 0.05	4.07 ± 0.05	3.85 ± 0.03	1/8/8/8
Gl213	05:42:09	+12:29:23	171.6 ± 4.0	H	M4.0	11.6 ± 0.01	7.12 ± 0.02	6.63 ± 0.02	6.39 ± 0.02	3/7/7/7
Gl229	06:10:34	-21:51:53	173.8 ± 1.0	H	M1.0	8.1 ± 0.02	5.06 ± 0.02	4.36 ± 0.02	4.16 ± 0.02	1/9/9/9
HIP31293	06:33:43	-75:37:47	110.9 ± 2.2	H	M2.5	10.3 ± 0.01	6.72 ± 0.02	6.15 ± 0.03	5.86 ± 0.02	3/7/7/7
HIP31292	06:33:47	-75:37:30	114.5 ± 3.2	H	M3.0	11.4 ± 0.01	7.41 ± 0.03	6.85 ± 0.03	6.56 ± 0.02	3/7/7/7
Gl250B	06:52:18	-05:11:24	114.8 ± 0.4	H	M2.0	10.1 ± 0.01	6.58 ± 0.03	5.98 ± 0.06	5.72 ± 0.04	5/7/7/7
Gl273	07:27:24	+05:13:30	263.0 ± 1.4	H	M3.5	9.9 ± 0.02	5.71 ± 0.03	5.22 ± 0.06	4.86 ± 0.02	1/7/7/7
Gl300	08:12:41	-21:33:12	125.8 ± 1.0	H	M4.0	12.1 ± 0.01	7.60 ± 0.02	6.96 ± 0.03	6.71 ± 0.03	2/7/7/7
GJ2066	08:16:08	+01:18:11	109.6 ± 1.5	H	M2.0	10.1 ± 0.02	6.62 ± 0.03	6.04 ± 0.03	5.77 ± 0.02	1/7/7/7
Gl341	09:21:38	-60:16:53	95.6 ± 0.9	H	M0.5	9.5 ± 0.02	6.44 ± 0.02	5.79 ± 0.03	5.59 ± 0.02	1/7/7/7
GJ1125	09:30:44	+00:19:18	103.5 ± 3.9	H	M3.0	11.7 ± 0.02	7.70 ± 0.02	7.18 ± 0.03	6.87 ± 0.02	1/7/7/7
Gl357	09:36:02	-21:39:42	110.8 ± 1.9	H	M2.5	10.9 ± 0.02	7.34 ± 0.03	6.74 ± 0.03	6.47 ± 0.02	1/7/7/7
Gl358	09:39:47	-41:04:00	105.6 ± 1.6	H	M3.0	10.7 ± 0.02	6.90 ± 0.03	6.32 ± 0.05	6.06 ± 0.02	1/7/7/7
Gl367	09:44:30	-45:46:36	101.3 ± 3.2	H	M1.5	10.0 ± 0.02	6.63 ± 0.02	6.04 ± 0.04	5.78 ± 0.02	1/7/7/7
Gl382	10:12:17	-03:44:47	127.1 ± 1.9	H	M2.0	9.3 ± 0.02	5.89 ± 0.02	5.26 ± 0.02	5.01 ± 0.02	1/7/7/7
Gl393	10:28:55	+00:50:23	141.5 ± 2.2	H	M2.0	9.6 ± 0.02	6.18 ± 0.02	5.61 ± 0.03	5.31 ± 0.02	1/7/7/7
Gl413.1	11:09:31	-24:36:00	93.0 ± 1.7	H	M2.0	10.4 ± 0.02	6.95 ± 0.02	6.36 ± 0.04	6.10 ± 0.02	1/7/7/7
Gl433	11:35:27	-32:32:23	112.6 ± 1.4	H	M1.5	9.8 ± 0.02	6.47 ± 0.02	5.86 ± 0.04	5.62 ± 0.02	1/7/7/7
Gl438	11:43:20	-51:50:23	119.0 ± 10.2	R	M1.5	10.4 ± 0.04	7.14 ± 0.02	6.58 ± 0.04	6.32 ± 0.02	2/7/7/7
Gl447	11:47:44	+00:48:16	299.6 ± 2.2	H	M4.0	11.1 ± 0.01	6.50 ± 0.02	5.95 ± 0.02	5.65 ± 0.02	3/7/7/7
Gl465	12:24:53	-18:14:30	113.0 ± 2.5	H	M2.0	11.3 ± 0.02	7.73 ± 0.02	7.25 ± 0.02	6.95 ± 0.02	1/7/7/7
Gl479	12:37:53	-52:00:06	103.2 ± 2.3	H	M3.0	10.7 ± 0.02	6.86 ± 0.02	6.29 ± 0.03	6.02 ± 0.02	1/7/7/7
Gl514	13:30:00	+10:22:36	130.6 ± 1.1	H	M1.0	9.0 ± 0.02	5.90 ± 0.02	5.30 ± 0.03	5.04 ± 0.03	1/7/7/7
Gl526	13:45:44	+14:53:30	185.5 ± 1.1	H	M1.0	8.4 ± 0.02	5.24 ± 0.05	4.65 ± 0.05	4.42 ± 0.02	1/8/8/7
Gl536	14:01:03	-02:39:18	98.3 ± 1.6	H	M1.0	9.7 ± 0.02	6.52 ± 0.02	5.93 ± 0.04	5.68 ± 0.02	1/7/7/7
Gl551	14:29:43	-62:40:47	771.6 ± 2.6	H	M5.0	11.0 ± 0.01	5.36 ± 0.02	4.83 ± 0.06	4.31 ± 0.03	3/7/7/8
Gl555	14:34:17	-12:31:06	165.0 ± 3.3	H	M4.0	11.3 ± 0.02	6.84 ± 0.02	6.26 ± 0.04	5.94 ± 0.03	1/7/7/7
Gl569A	14:54:29	+16:06:04	101.9 ± 1.7	H	M3.0	10.4 ± 0.05	6.63 ± 0.02	5.99 ± 0.02	5.77 ± 0.02	6/7/7/7
Gl581	15:19:26	-07:43:17	160.9 ± 2.6	H	M3.0	10.6 ± 0.01	6.71 ± 0.03	6.09 ± 0.03	5.84 ± 0.02	3/7/7/7
Gl588	15:32:13	-41:16:36	168.7 ± 1.3	H	M2.5	9.3 ± 0.02	5.65 ± 0.02	5.03 ± 0.02	4.76 ± 0.02	1/7/7/7
Gl618A	16:20:04	-37:31:41	119.8 ± 2.5	H	M3.0	10.6 ± 0.02	6.79 ± 0.02	6.22 ± 0.02	5.95 ± 0.02	1/7/7/7
Gl628	16:30:18	-12:39:47	233.0 ± 1.6	H	M3.5	10.1 ± 0.02	5.95 ± 0.02	5.37 ± 0.04	5.08 ± 0.02	1/7/7/7
Gl667C	17:18:58	-34:59:42	146.3 ± 9.0	H	M2.0	10.3 ± 0.04	6.85 ± 0.02	6.32 ± 0.04	6.04 ± 0.02	2/7/7/7
Gl674	17:28:40	-46:53:42	220.2 ± 1.4	H	M2.5	9.4 ± 0.02	5.71 ± 0.02	5.15 ± 0.03	4.86 ± 0.02	1/7/7/7
Gl678.1A	17:30:22	+05:32:53	100.2 ± 1.1	H	M1.0	9.3 ± 0.01	6.24 ± 0.02	5.65 ± 0.04	5.42 ± 0.03	3/7/7/7
Gl680	17:35:13	-48:40:53	102.8 ± 2.8	H	M2.0	10.1 ± 0.02	6.67 ± 0.02	6.08 ± 0.03	5.83 ± 0.02	1/7/7/7
Gl682	17:37:03	-44:19:11	196.9 ± 2.1	H	M3.5	10.9 ± 0.02	6.54 ± 0.02	5.92 ± 0.04	5.61 ± 0.02	1/7/7/7
Gl686	17:37:53	+18:35:30	123.0 ± 1.6	H	M1.5	9.6 ± 0.02	6.36 ± 0.02	5.79 ± 0.02	5.57 ± 0.02	1/7/7/7
Gl693	17:46:35	-57:19:11	171.5 ± 2.3	H	M3.0	10.8 ± 0.02	6.86 ± 0.02	6.30 ± 0.04	6.02 ± 0.02	1/7/7/7
Gl699	17:57:49	+04:41:36	549.0 ± 1.6	H	M3.5	9.5 ± 0.02	5.24 ± 0.02	4.83 ± 0.03	4.52 ± 0.02	1/7/7/7
Gl701	18:05:07	-03:01:53	128.9 ± 1.4	H	M1.0	9.4 ± 0.02	6.16 ± 0.02	5.57 ± 0.04	5.31 ± 0.02	1/7/7/7
Gl752A	19:16:55	+05:10:05	170.4 ± 1.0	H	M2.0	9.1 ± 0.02	5.58 ± 0.03	4.93 ± 0.03	4.67 ± 0.02	1/7/7/7
Gl832	21:33:34	-49:00:36	201.9 ± 1.0	H	M1.5	8.7 ± 0.02	5.36 ± 0.02	4.69 ± 0.02	4.47 ± 0.02	1/9/9/9
Gl846	22:02:10	+01:24:00	97.6 ± 1.5	H	M0.5	9.1 ± 0.02	6.20 ± 0.02	5.56 ± 0.05	5.32 ± 0.02	1/7/7/7
Gl849	22:09:40	-04:38:30	109.9 ± 2.1	H	M3.0	10.4 ± 0.02	6.51 ± 0.02	5.90 ± 0.04	5.59 ± 0.02	1/7/7/7
Gl876	22:53:17	-14:15:48	213.3 ± 2.1	H	M3.5	10.2 ± 0.02	5.93 ± 0.02	5.35 ± 0.05	5.01 ± 0.02	1/7/7/7
Gl877	22:55:46	-75:27:36	116.1 ± 1.2	H	M2.5	10.4 ± 0.02	6.62 ± 0.02	6.08 ± 0.03	5.81 ± 0.02	1/7/7/7
Gl880	22:56:35	+16:33:12	146.1 ± 1.0	H	M1.5	8.6 ± 0.02	5.36 ± 0.02	4.75 ± 0.05	4.52 ± 0.02	1/7/8/7
Gl887	23:05:52	-35:51:12	303.9 ± 0.9	H	M1.0	7.3 ± 0.01	4.17 ± 0.05	3.61 ± 0.05	3.36 ± 0.03	3/8/8/8
Gl908	23:49:13	+02:24:06	167.3 ± 1.2	H	M1.0	9.0 ± 0.01	5.83 ± 0.02	5.28 ± 0.03	5.04 ± 0.02	3/7/7/7
LTT9759	23:53:50	-75:37:53	100.1 ± 1.1	H	M2.5	10.0 ± 0.02	6.45 ± 0.02	5.78 ± 0.02	5.55 ± 0.03	1/7/7/7

references: H – (van Leeuwen 2007); H06 – Henry et al. (2006); R – Reid et al. (1995); 1– Koen et al. (2010); 2 – Henden et al. (2009, 2012); 3 – Perryman et al. (1997); 4 – Weis (1993); 5 – Laing (1989); 6 – Fabricius et al. (2002); 7 – Skrutskie et al. (2006); 8 – Leggett (1992).

stars have a very low photometric period (2.2 and 2.9 days respectively) and are very active ($\log L_{H_\alpha}/L_{bol}$ of -3.8 and -3.77 respectively) despite having a low value of $v \sin i$. Gl803, on the other hand is a very young star (20 Myr) with a circumstellar disk (Kalas et al. 2004). Therefore, it belongs in the same 'high

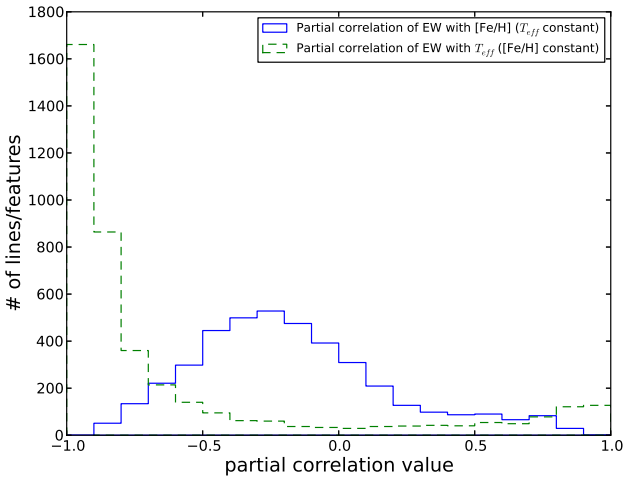

Fig. 2. Histograms of the partial correlations of [Fe/H] (solid blue histogram) and T_{eff} (dashed green histogram).

rotation/low $v \sin i$' group as the other two stars. Our final sample has 58 stars, as shown in Table 1.

Then we did a least squares linear fit of the EWs with the metallicity and effective temperature. The reference values were calculated with the calibration of Neves et al. (2012), for [Fe/H], and with the three ($V-J$, $V-H$, and $V-K_S$) photometric calibrations of Casagrande et al. (2008), for T_{eff}, where we took the average value. From each line/feature i of every star m we calculate a EW value. Then we have

$$W_{i,m} = \alpha_i [Fe/H]^T_m + \beta_i T^T_{eff,m} + \gamma_i, \quad (2)$$

where $W_{i,m}$ is a $i \times m$ matrix containing the EWs, and both $[Fe/H]^T_m$, and T^T_{effm} are the transpose matrices of the parameter values and are, therefore, $1 \times m$ vectors. The α and the β are the coefficients related to metallicity and effective temperature, respectively, while γ is an independent coefficient. The error associated to each parameter p is calculated as

$$\epsilon_p = \sqrt{RSS.J}, \quad (3)$$

where RSS is the residual sum of squares, expressed as

$$RSS = \frac{\sum (x_{i,model} - x_i)^2}{n_{obs} - n_{coef}}, \quad (4)$$

and J is the diagonal of the estimate of the jacobian matrix around the solution. The $x_{i,model}$, x_i, n_{obs}, and n_{coef} from Eq. 3 are, respectively, the predicted value of the data, x_i, by the regression model, the data values, the number of data points, and the number of coefficients. We assume that both metallicity and effective temperature are independent and do not correlate with each other. This assumption was tested by perturbing each parameter in turn by introducing an positive or negative offset and then calculating both parameters. There was no difference in the obtained values of the unperturbed parameter. We also tried to use the full covariance matrix to calculate the uncertainties but in the end we got a worse result for the dispersion of the calibration. Therefore, we decided to use only the diagonal values of the covariance matrix. The total error of the coefficients associated to each line i can then be written as

$$\epsilon_i = \sqrt{\epsilon^2_\alpha + \epsilon^2_\beta + \epsilon^2_\gamma}. \quad (5)$$

The aim of the calibration is to increase the precision of both [Fe/H] and T_{eff} determinations. To do that we need to obtain the values of the metallicity and effective temperature via a weighted least squares refit, that is obtained after a left multiplication of $(C^T_{3,i} C_{i,3})^{-1} C^T_{3,i}$ on both terms of Eq. 2, where C is the calibration matrix or the coefficient matrix, that can be written as

$$C_{i,3} = \begin{bmatrix} \alpha_{1,1} & \beta_{1,2} & \gamma_{1,3} \\ \alpha_{2,1} & \beta_{2,2} & \gamma_{2,3} \\ \dots & \dots & \dots \\ \alpha_{i,1} & \beta_{i,2} & \gamma_{i,3} \end{bmatrix}, \quad (6)$$

and C^T is the transpose of C. The refit is then expressed, for each star m, as

$$\begin{bmatrix} [Fe/H] \\ T_{eff} \\ Ind \end{bmatrix} = (C^T_{3,i} C_{i,3})^{-1} C^T_{3,i} W_{i,m}, \quad (7)$$

where Ind is the value of the independent parameter. Finally we introduce a weight to Eq. 7, using a *Levenberg-Marquardt* (Press et al. 1992) algorithm. The normalised weight E_i is defined as

$$E_i = \frac{1/\epsilon^2_i}{\sum 1/\epsilon^2_i}. \quad (8)$$

Other methods were tested, such as choosing lines/features with the best correlations or partial correlations with the parameters. However, the weighted least squares approach performed best at minimising the uncertainties of both metallicity and temperature.

Quantitatively we obtain a dispersion of 0.07 dex for the metallicity and 100K for the effective temperature, as shown in Fig. 3. The calibration is valid between -0.91 to 0.25 dex for [Fe/H], 2600 to 3800 K for T_{eff}, and between M0 to M5.5, considering a ± 0.5 uncertainty in the spectral type. Our dispersion is described by the root mean square error (RMSE), and defined as

$$RMSE = \sqrt{\frac{\sum (x_i - x_{ref})^2}{n_{obs} - n_{coef}}}, \quad (9)$$

where x_i is the estimated quantity, x_{ref} the reference value for the same quantity, n_{obs} the number of calibrators and n_{coef} the number of parameters used in the calibration (three in this case).

The calculated parameters as well as the reference determinations for [Fe/H] and T_{eff} are listed in Table 2. Columns 1 and 3 contain the values for the reference calibrations, while columns 2 and 4 show the values obtained with our new calibration. We emphasise here that we only get an improvement on the precision. The accuracy of the calibration as well as its systematics are tied to the original determinations of the parameters.

2.2. Estimation of the calibration uncertainties

To validate our calibration and have a better understanding of the uncertainties of our measurements we performed a bootstrap resampling and calculated the root mean square error of validation ($RMSE_V$) of our calibration.

The bootstrap method we implemented tests how the *rms* of the calibration changes when using slightly different 'bootstrapped' samples. To have a statistical significative number we first created 10.000 virtual samples by randomly drawing with

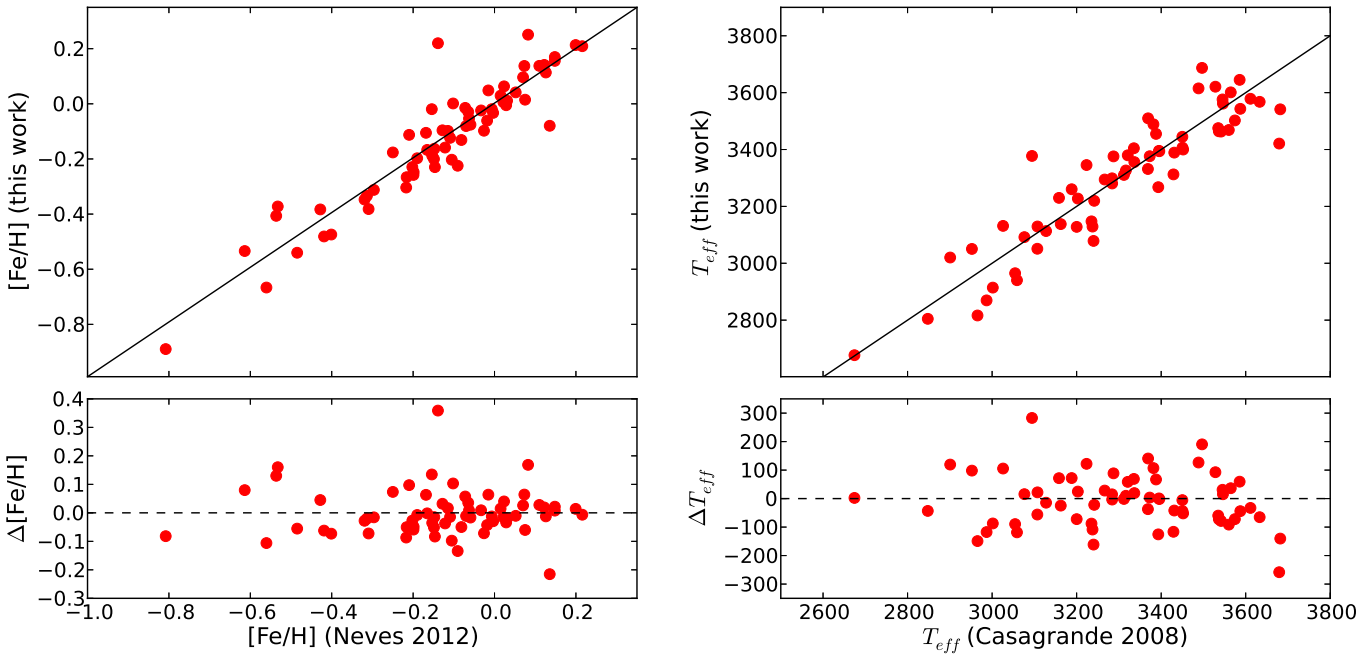

(a) (b)

Fig. 3. (a) [Fe/H] comparison between this work and the photometric calibration of Neves et al. (2012); (b) T_{eff} comparison between this work and the photometric calibration of Casagrande et al. (2008).

repetition, for each virtual sample, a number of stars equal to the size of our sample. The random drawing followed a random uniform distribution. Then we calculated the *rms* for each trial and measured the 1σ Gaussian equivalent interval between 15.9% and 84.1% from the resulting distribution, following the procedure of e.g. Burgasser et al. (2003); Neves et al. (2013). The distributions of the *rms* for both parameters are depicted in Fig. 4. The final result shows a variation of the *rms* of the [Fe/H] and T_{eff} by ±0.01 dex and ±13 K respectively.

The calculation of the RMSE_V is a predicted residual sum of squares (PRESS) procedure (Weisberg 2005) and follows the description in the Appendix of Rojas-Ayala et al. (2012). In short, we try to obtain the original value of the metallicity and temperature of each star *i* of the calibration leaving that star out when calculating the calibration. Then, we calculate the residuals, or

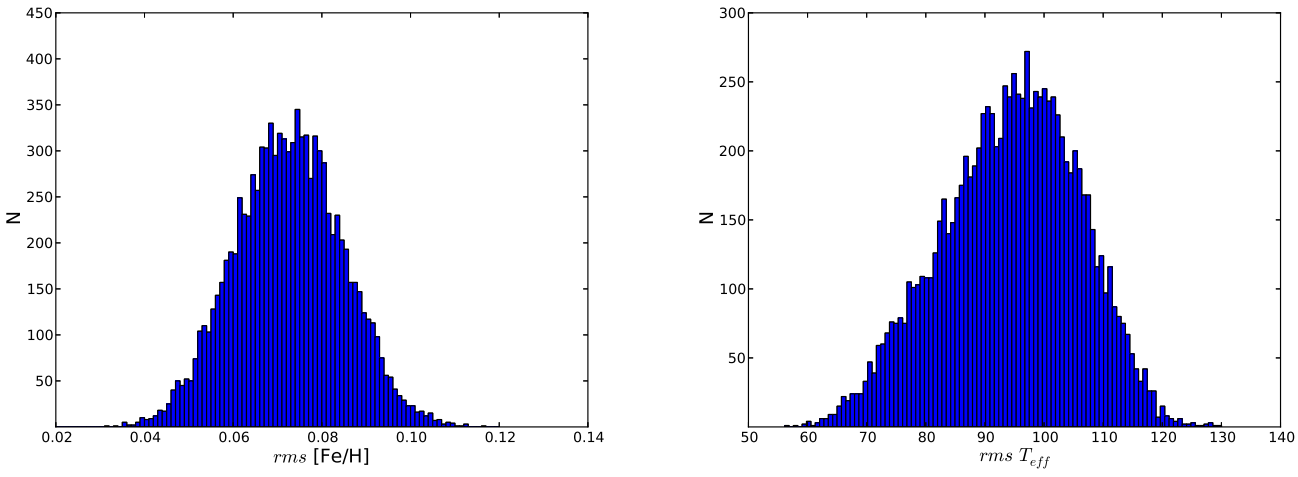

(a) (b)

Fig. 4. Histogram of the dispersion given by bootstrap for [Fe/H] (a) and T_{eff} (b). The N is the number of trials.

Table 2. Calibration sample table with the reference and calibrated metallicity and effective temperature. Sorted by right ascension.

star	$[Fe/H]_{N12}$ [dex]	$[Fe/H]_{NEW}$ [dex]	T_{effC08} [[K]	T_{effNEW} [K]
Gl1	-0.42	-0.48	3528	3612
Gl54.1	-0.43	-0.40	2901	2997
Gl87	-0.32	-0.34	3565	3601
Gl105B	-0.15	-0.04	3054	2958
LP771-95A	-0.53	-0.38	3393	3261
Gl176	-0.00	-0.01	3369	3355
Gl191	-0.81	-0.91	3679	3389
Gl205	0.15	0.25	3497	3768
Gl213	-0.21	-0.13	3026	3120
Gl229	-0.06	0.01	3586	3700
HIP31293	-0.06	-0.07	3312	3319
HIP31292	-0.13	-0.10	3158	3236
Gl250B	-0.11	-0.10	3369	3526
Gl273	-0.07	-0.04	3107	3122
Gl300	0.07	0.11	2965	2809
GJ2066	-0.11	-0.19	3388	3466
Gl341	-0.17	-0.11	3633	3613
GJ1125	-0.17	-0.12	3162	3134
Gl357	-0.31	-0.33	3335	3406
Gl358	-0.01	-0.02	3240	3088
Gl367	-0.11	-0.08	3452	3418
Gl382	0.02	0.04	3429	3348
Gl393	-0.15	-0.22	3396	3409
Gl413.1	-0.08	-0.11	3373	3395
Gl433	-0.15	-0.17	3450	3472
Gl438	-0.54	-0.39	3536	3475
Gl447	-0.25	-0.20	2952	3036
Gl465	-0.56	-0.67	3382	3467
Gl479	0.03	-0.00	3238	3143
Gl514	-0.15	-0.15	3574	3537
Gl526	-0.20	-0.23	3545	3583
Gl536	-0.15	-0.13	3546	3586
Gl551	0.08	-0.01	2674	2649
Gl555	0.11	0.11	2987	2865
Gl569A	0.14	-0.06	3235	3165
Gl581	-0.20	-0.24	3203	3232
Gl588	0.05	0.05	3284	3320
Gl618A	-0.07	-0.08	3242	3227
Gl628	-0.06	-0.05	3107	3050
Gl667C	-0.48	-0.54	3431	3388
Gl674	-0.20	-0.26	3284	3285
Gl678.1A	-0.12	-0.10	3611	3623
Gl680	-0.09	-0.20	3395	3411
Gl682	0.07	0.07	3002	2907
Gl686	-0.31	-0.36	3542	3476
Gl693	-0.30	-0.32	3188	3251
Gl699	-0.61	-0.55	3094	3356
Gl701	-0.22	-0.27	3535	3497
Gl752A	0.01	0.04	3336	3376
Gl832	-0.19	-0.18	3450	3430
Gl846	-0.10	0.08	3682	3613
Gl849	0.22	0.20	3200	3143
Gl876	0.12	0.11	3059	2939
Gl877	-0.03	-0.03	3266	3304
Gl880	0.03	0.07	3488	3666
Gl887	-0.22	-0.24	3560	3491
Gl908	-0.40	-0.47	3587	3534
LTT9759	0.15	0.18	3316	3354

the difference between the original and obtained value for each star and add them up in quadrature. The PRESS statistic is then defined as

$$PRESS = \sum (y_i - y_{ref})^2, \tag{10}$$

where y_i is the estimated value of the parameter and y_{ref} is the reference value of the measured quantity. From here we can calculate the root mean squared error of validation,

$$RMSE_V = \sqrt{\frac{PRESS}{n_V}}, \tag{11}$$

where n_V is the number of calibrators. The $RMSE_V$ value can then be used to obtain confidence intervals. We obtain a $RMSE_V$ value of 0.08 dex and $\sim$ 300 K for the [Fe/H] and T_{eff} respectively and will use these values as our 1σ confidence intervals, assuming a normal cumulative distribution function. Discuss last phrase. Babs?. Table 3 summarises our results.

Table 3. Uncertainty estimators for [Fe/H] and T_{eff}.

Estimator	[Fe/H] [dex]	T_{eff} [K]
RMSE	0.07	100
Bootstrap	0.07±0.01	100±20
$RMSE_V$	0.08	300

We observe that the uncertainties calculated with the different techniques are consistent with each other. The uncertainty for T_{eff} is large but is in line with the expected uncertainties. We also perturbed our calibration by introducing an offset in [Fe/H] or T_{eff}, as explained in Sect. 2.1. We concluded that an introduction of a fixed quantity on either parameter does not affect the measurement of the other.

2.3. Testing the calibration as a function of resolution and SNR

We also calculated the dispersion of the parameters as a function of the resolution and SNR. The resolution of the HARPS spectra was degraded by means of a convolution between the spectra and a normalised gaussian curve, simulating the instrumental profile, with $FWHM = \lambda/R$, where λ is the wavelength and R the resolution we intend to obtain. From here, the standard deviation of the gaussian is calculated with the well known formula

$$\sigma = \frac{FWHM}{2\sqrt{2\log 2}}. \tag{12}$$

The desired signal to noise ratio was obtained by introducing random gaussian noise in the spectra. The σ and the noise were adjusted to the HARPS resolution ($R \sim 115.000$) and to the original SNR @ 5500Å of each spectrum Should we use here a longer wavelength reference?. The final values for both parameters are

$$\sigma' = \sqrt{\sigma^2 - \sigma^2_{HARPS}}, \tag{13}$$

and

$$noise' = \sqrt{noise^2 - noise^2_{HARPS}}. \tag{14}$$

Figures 5 and 6 show the residuals as a function of resolution (while SNR is kept constant at 100) and as a function of SNR

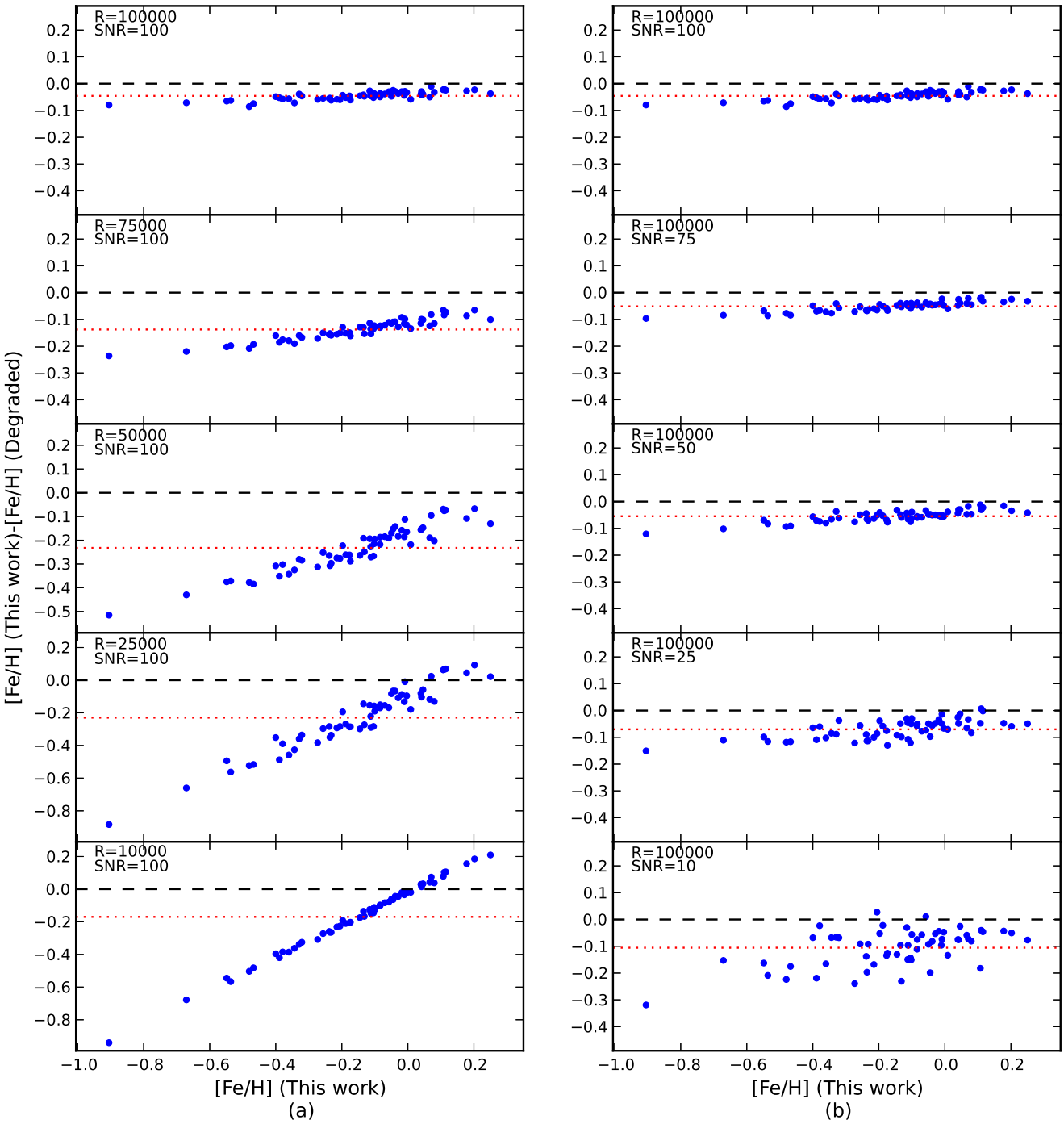

Fig. 5. Difference of the [Fe/H] for this work and the [Fe/H] calculated with different resolution/SNR combinations as a function of the resolution and SNR.

(while the resolution is kept constant at 100.000) for [Fe/H] and T_{eff} respectively. The red dotted line depicts the offset of the residuals.

We observe in both Figures the existence of different trends for different resolutions and SNR. To correct these trends we performed a linear fit for each Resolution/SNR combination with the functional form [Fe/H](This work)= a.[Fe/H](Degraded)+b for metallicity, and T_{eff}(This work)= a.T_{eff}(Degraded)+b for effective temperature. The values for each combination are shown in Table 4.

From here we calculated the dispersion of the difference between the corrected parameter values and the ones obtained from our original calibration, and added this dispersion with the one from our calibration in quadrature. Table 5 shows the results. The horizontal header of both tables correspond to the SNR of the spectra, between 100 and 10, while the vertical header de-

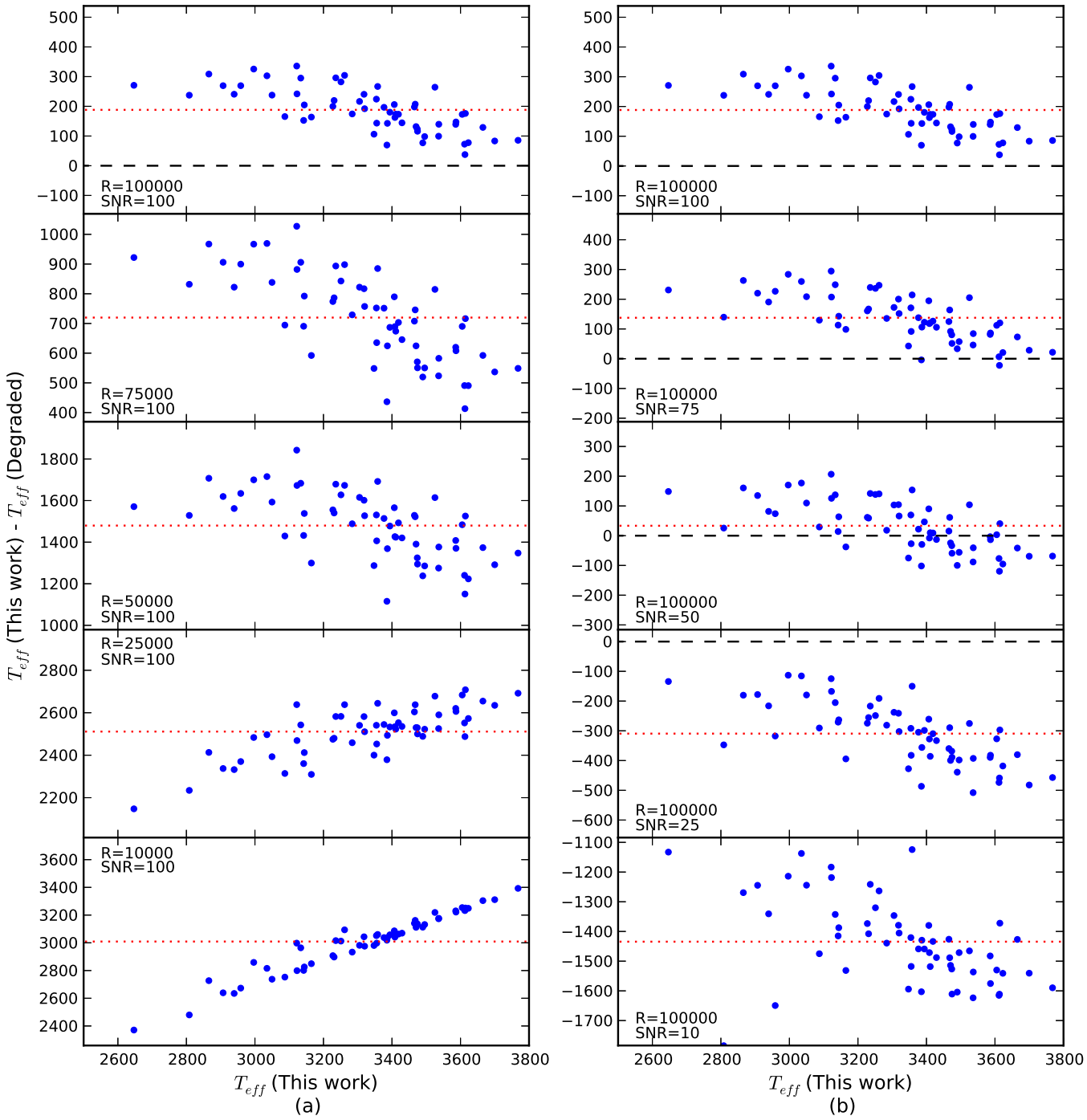

Fig. 6. Difference of the [Fe/H] for this work and the [Fe/H] calculated with different resolution/SNR combinations as a function of the resolution and SNR.

picts their resolution, from 100.000 to 10.000. The row with the resolution number is the value of the dispersion of the calibration using the corresponding resolution/snr combination. The rows with the suffix *res* show the dispersion of the difference between the values of our calibration and the ones obtained with the corrected values for each resolution/snr combination.

From Table 5 and Figs. 5 and 6 we observe that, as the resolution degrades, the dispersion and offset of the residuals increase. In the case of [Fe/H], the dispersion value holds well for resolution and SNR higher and equal to 50.000 and 25, respectively.Below $R = 50.000$ we consider that the calibration has a value of dispersion that is too high and therefore cannot be applied. Regarding T_{eff}, we consider that the calibration is valid for the same resolution and SNR intervals as in [Fe/H]. Table 5 may be used as a guideline for the uncertainties of the parameters when using spectra other than HARPS. The increasing

Table 4. Linear fit coefficients *a* and *b* from the relation between the values of the parameters of this work calibration and the values calculated for different combinations of resolution and SNR.

(a) [Fe/H]

SNR	100		75		50		25		10	
Resolution	a	b	a	b	a	b	a	b	a	b
100000	1.0582	-0.0394	1.0705	-0.0443	1.0796	-0.0471	1.0956	-0.0624	1.0910	-0.1013
75000	1.1894	-0.1353	1.2101	-0.1362	1.2113	-0.1396	1.2727	-0.1520	1.1727	-0.1749
50000	1.5908	-0.2804	1.6063	-0.2848	1.6390	-0.2843	1.6140	-0.2792	1.3489	-0.2667
25000	1.9301	-0.3021	1.8556	-0.2900	1.7552	-0.2787	1.7526	-0.2667	0.9696	-0.2119
10000	0.7717	-0.1656	1.3339	-0.1747	2.0107	-0.1881	1.0431	-0.1774	0.7522	-0.1860

(b) T_{eff}

SNR	100		75		50		25		10	
Resolution	a	b	a	b	a	b	a	b	a	b
100000	0.7957	829.0747	0.7865	818.5115	0.7764	769.6886	0.7312	667.9319	0.6666	152.6770
75000	0.6336	1674.7330	0.6389	1624.5838	0.6454	1526.6327	0.6485	1265.5323	0.6181	618.0058
50000	0.6284	2165.7729	0.6511	2081.6257	0.6667	1955.7645	0.6979	1581.2159	0.6813	740.3490
25000	1.2686	2292.4712	1.3430	2120.1743	1.3703	1864.6764	1.2981	1279.5182	1.0348	222.7126
10000	2.2880	2601.2130	3.5903	1815.5954	3.2029	1357.7898	1.2830	1835.07950	0.6124	1713.3062

Table 5. Dispersion of the residuals of the parameters as a function of the resolution and SNR.

(a) [Fe/H]

SNR	100	75	50	25	10
Resolution					
100000	0.071	0.071	0.071	0.076	0.098
100000res	0.010	0.010	0.013	0.030	0.068
75000	0.072	0.073	0.073	0.082	0.110
75000res	0.016	0.020	0.021	0.043	0.085
50000	0.087	0.092	0.100	0.113	0.140
50000res	0.052	0.060	0.072	0.089	0.121
25000	0.202	0.206	0.207	0.204	0.219
25000res	0.189	0.194	0.195	0.192	0.207
10000	0.235	0.235	0.233	0.233	0.230
10000res	0.224	0.224	0.222	0.222	0.219

(b) T_{eff}

SNR	100	75	50	25	10
Resolution					
100000	109	110	112	114	136
100000res	43	45	51	55	92
75000	121	120	121	124	142
75000res	68	66	68	73	101
50000	132	130	131	135	147
50000res	86	83	84	91	108
25000	148	145	146	163	192
25000res	109	105	106	129	164
10000	219	207	226	255	256
10000res	195	181	203	235	236

dispersions and offsets with the resolution should originate from the nature of our 'peak-to-peak technique' because it does not consider the continuum. As the resolution gets worse, more and more flux from the 'peak to peak' region is lost to the line wings. Moreover, as the resolution decreases there is an increase of line blending that makes the measurement of the correct flux of the each line/feature increasingly difficult.

3. Comparison with the literature

A comparison with other studies in the literature was performed. This comparison allow us to have a measure of the accuracy of our calibration and the possible systematics that it may suffer. The results are shown in Table 6. The results for [Fe/H] are separated by photometric and spectroscopic techniques. The first column depicts the name of the calibration along with its reference. Column two and three describe the dispersion and offset. The last column reports the number of stars in common with our sample.

Table 6. Dispersion and offset of [Fe/H] and T_{eff} from the residuals of our calibration against other studies. The last column shows the number of stars in common.

Photometric [Fe/H] calibrations	*rms*	offset	N
B05 (Bonfils et al. 2005)	0.10	-0.04	58
SL10 (Schlaufman & Laughlin 2010)	0.11	0.03	58
J12 (Johnson et al. 2012)	0.20	0.09	58
Spectroscopic [Fe/H] calibrations	*rms*	offset	N
All calibrations	0.12	0.06	38
RA12 (Rojas-Ayala et al. 2012)	0.12	0.05	15
T_{eff} calibrations	*rms*	offset	N
RA12 (Rojas-Ayala et al. 2012)	293	230	15
O12 (Önehag et al. 2012)	143	51	6
BO12 (Boyajian et al. 2012)	161	123	44
M13b (Mann et al. 2013b)	150	92	6
R13 (Rajpurohit et al. 2013a)	150	117	9

The photometric [Fe/H] was calculated with the relations of Bonfils et al. (2005), Schlaufman & Laughlin (2010) and Johnson et al. (2012) (hereafter B05, SL10, and J12, while the spectroscopic [Fe/H] was taken directly from the works of Rojas-Ayala et al. (2012), Önehag et al. (2012), Terrien et al. (2012), Newton (2013), and Mann et al. (2013b) (hereafter RA12,O12,T12, EN13, and M13b respectively), except in the case of Mann et al. (2013a) (hereafter M13), where the values of

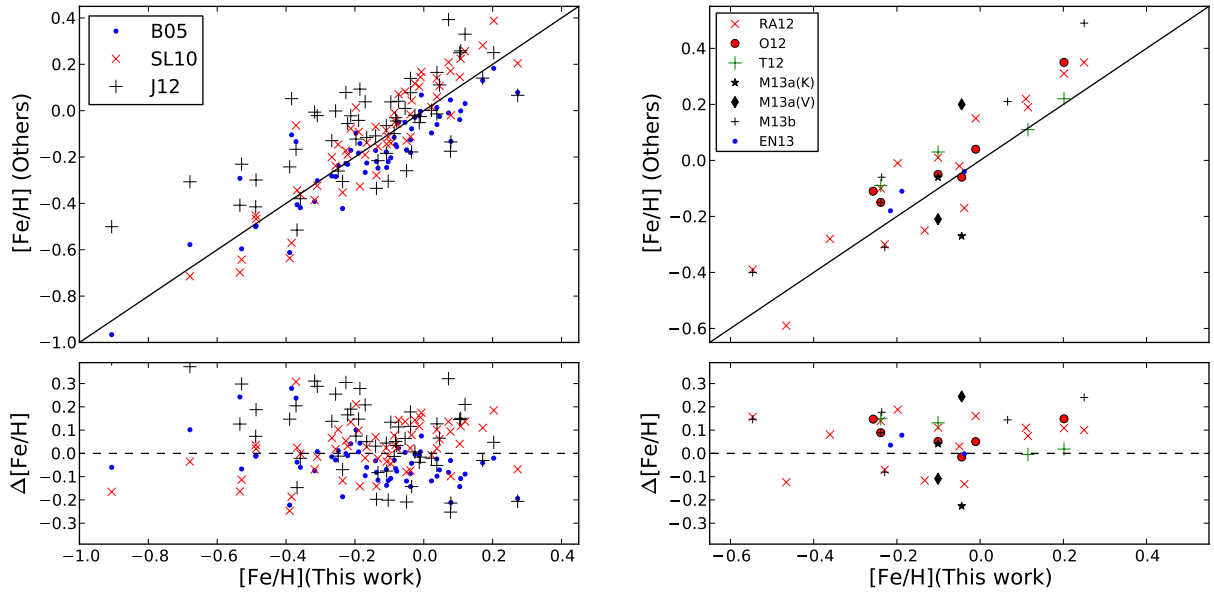

(a) (b)

Fig. 7. *Upper panel:* [Fe/H]-[Fe/H] plots comparing the values of this work against others in the literature. The plot (a) shows the results of our work versus three photometric calibrations taken from the literature, while plot (b) depicts the comparison between our results against other works.The solid black line of both (a) and (b) depict the identity line;*Lower panel:* Comparison plot residuals. The dashed black line marks the zero point of our calibration.

the visible (their Eq. 8) and K-band (their Eq. 16) calibrations were provided directly by the author.

Figure 7 shows two [Fe/H]-[Fe/H] plots. The left plot (a) shows the comparison of our results with the works based on photometric scales. The blue dots, red crosses and black plus signs indicate the results of B05, SL10, and J12 respectively. The right plot (b) depicts the comparison of our work with other spectroscopic calibrations. The red crosses, red circles, green plus signs, black stars, diamonds, and pluses and blue dots correspond to the measurements of RA12, O12, T12, M13, M13b, and EN13 respectively. The (K) and (V) in M13 correspond to measurements performed with a V- and K-band calibration respectively. The solid black line in the upper panel of both plots defines an identity line. The lower panels show the residuals. The dashed black line marks the zero-point of the calibration.

Regarding the effective temperature, the photometric temperature scale of Boyajian et al. (2012) (hereafter BO12) was calculated using the average value of the three colour-metallicity T_{eff} relations ($V-J$, $V-H$, and $V-K_S$) from their Table 9, and imposed a cutoff of $V-K < 4.5$ for the three scales, according to their limits. The T_{eff} values of RA12, O12, M13, M13b, and Rajpurohit et al. (2013a) (hereafter R13) were taken directly from their works. Figure 8 describes the comparison between our T_{eff} results and those of the other authors. The solid black in the upper panel line defines an identity line. The lower panels show the residuals.

.

We also calculated linear fits for the three T_{eff} scales of BO12, RA12, and R13 where we consider we have enough stars in common. For the BO12 the relation is

$$T_{eff} = (1.078 \pm 0.144)T_{eff,B12} - 401.961 \pm 511.704, \quad (15)$$

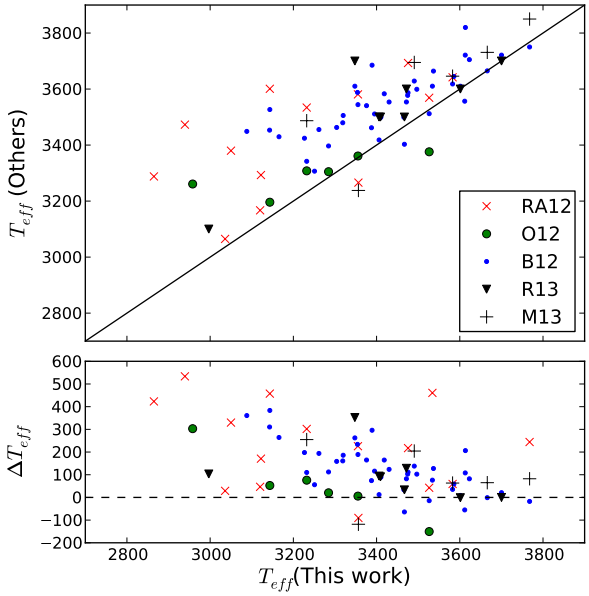

Fig. 8. *Upper panel:* T_{eff}-T_{eff} plot comparing the values of this work against others in the literature. The solid black line depicts the identity line;*Lower panel:* Comparison plot residuals. The dashed black line marks the zero point of our calibration.

for RA12,

$$T_{eff} = (0.731 \pm 0.176)T_{eff,RA12} + 712.216 \pm 617.706, \quad (16)$$

and for R13,

$$T_{eff} = (1.106 \pm 0.158)T_{eff,R13} - 481.857 \pm 545.780 \quad (17)$$

The photometric [Fe/H] measurements as well as the T_{eff} determinations using the calibration of B12 were calculated with the data from Table 1.

For metallicity we observe a general agreement between our results and the ones from the literature. We note here that the calibration of SL10 is very similar to our reference calibration, from Neves et al. (2012), and this is the reason why we obtain a value of dispersion smaller than the one of the original calibration (0.11 vs 0.17 dex). The dispersion of the oldest photometric calibration B05 is surprisingly low, considering that the original dispersion for this calibration is 0.20 dex. Regarding the J12 calibration, we obtain a *rms* of 0.20 dex, higher that their reported value of 0.15 dex. The dispersion of the spectroscopic calibrations are within the expected values (0.12 dex). The offset is smaller than the dispersion value of our calibration. We combined all spectroscopic calibrations due to a lack of stars in common but we also show the results of RA12 separately, where we have 15 data points.

Regarding T_{eff} we observe a good agreement with the latest results from R13 using the latest BT-SETTL models. In fact, if we remove the outlier star GJ 382, we obtain a *rms* of 116 K and an offset of 87 K, practically within the uncertainties of the R13 determinations. However we also observe considerable dispersion and offset with both RA12 and BO12 comparison samples. The BO12 determination tend to converge with ours as the T_{eff} increases. We also note a systematic underestimation of our values of temperature in general that increases below 3200K. The O12 determinations have the smallest scatter and offset, but this result is expected since they use the same reference T_{eff} calibration as we do.

3.1. Using the calibration

The code of the calibration is written in python 2.7 and can be downloaded at http://www.astro.up.pt/resources/mcal. The program is very simple to use. The first step is to write the filenames of your spectra into *stars.txt*, replacing the two demonstration filenames, *Gl105B_S1D.fits* and *Gl849_S1D.fits*. Then, one just need to change the startup options, described in the startup section of the file *runallv1.py*. Depending on the resolution and SNR of the spectra, one should use the values of Table 5 as the reference of precision of [Fe/H] and T_{eff}.

The compressed zip file *calibration.zip* contains all the necessary files needed to run the calibration, as described in the following list:

- *runallv1.py* - script to run all the other programs. In the startup section one can choose to use FFT to filter high frequency noise, the file type of the input spectra (FITS or text file), and the name of the file with the full path of the spectra.
- *fft_filterv1.py* - function that performs the FFT filtering of the spectra. It takes 5-10 minutes per star to use this filter depending on CPU processing power.
- *int_calc_stars.py* - function to calculate the pseudo EWs of the relevant lines. It uses lines.rdb as input. An output file, ew_out.npz, is also created. It takes 3-5 minutes per star to calculate the EWs.
- *mcalv1.npz* - function that calculates the [Fe/H] and Teff of each star using the calibration matrix file *coef_cal.npz*. the output will be displayed on the screen and can also be optionally saved to a file (check the startup section of *runallv1.py* for details).
- *stars.txt* - text file with the full path of the spectra. This file should have all the spectra files for analysis.
- *Gl105B_S1D.fits* and *Gl849_S1D.fits* are two HARPS spectra that can be used to demonstrate how the program works. Their full file names appear in the file stars.txt. One should remove them from *stars.txt* before calibrating new stars.

4. Discussion

In this paper we present a new high-precision calibration for M dwarfs. We achieve a *rms* of 0.07 dex for metallicity and 100 K for effective temperature. Alternatively we obtain a $RMSE_V$ value of 0.08 dex for [Fe/H] and 300 K for T_{eff}. A bootstrap resampling was also conducted, showing a variation of the *rms* of [Fe/H] and T_{eff} of the order of ± 0.01 dex and ± 20 K respectively. Our calibration is available for download at http://www.astro.up.pt/resources/mcal. The procedure to use our calibration is detailed in this webpage. A test of the performance of the calibration as a function of the resolution and SNR was also performed. We conclude that the calibration behaves well down to R = 50.000 and SNR = 25, after correcting the observed trends.

To have a measure of the accuracy of our calibration, we tested it against several studies from the literature. Most studies agree well with our [Fe/H] determinations, and the offset is almost always below the precision of the calibration. For T_{eff} however, the same agreement could not be met. Despite reaching a very good agreement with the results of Rajpurohit et al. (2013a), that use synthetic spectra from the latest BT-SETTL models, the dispersion as well as the systematics between our calibration and the other works is considerable and beyond the calibration errors. Further studies are needed to investigate the nature of these systematics.

Acknowledgements. We acknowledge the support by the European Research Council/European Community under the FP7 through Starting Grant agreement number 239953. The financial support from the "Programme National de Planétologie" (PNP) of CNRS/INSU, France, is gratefully acknowledged. VN acknowledges the support from Fundação para a Ciência e a Tecnologia (FCT) of the fellowship SFRH/BD/60688/2009. NCS also acknowledges the support in the form of a Investigador FCT contract funded by Fundação para a Ciência e a Tecnologia (FCT) /MCTES (Portugal) and POPH/FSE (EC). This research has made use of the SIMBAD database, operated at CDS, Strasbourg, France, and of the Extrasolar Planet Encyclopaedia at exoplanet.eu. This publication makes use of data products from the Two Micron All Sky Survey, which is a joint project of the University of Massachusetts and the Infrared Processing and Analysis Center/California Institute of Technology, funded by the National Aeronautics and Space Administration and the National Science Foundation.

References

Allard, F., Homeier, D., & Freytag, B. 2011, in Astronomical Society of the Pacific Conference Series, Vol. 448, 16th Cambridge Workshop on Cool Stars, Stellar Systems, and the Sun, ed. C. Johns-Krull, M. K. Browning, & A. A. West, 91
Allard, F., Homeier, D., & Freytag, B. 2012, Royal Society of London Philosophical Transactions Series A, 370, 2765
Bean, J. L., Sneden, C., Hauschildt, P. H., Johns-Krull, C. M., & Benedict, G. F. 2006, ApJ, 652, 1604
Bonfils, X., Delfosse, X., Udry, S., et al. 2013, A&A, 549, A109
Bonfils, X., Delfosse, X., Udry, S., et al. 2005, A&A, 442, 635
Boyajian, T. S., von Braun, K., van Belle, G., et al. 2012, ApJ, 757, 112
Burgasser, A. J., Kirkpatrick, J. D., Reid, I. N., et al. 2003, ApJ, 586, 512
Casagrande, L., Flynn, C., & Bessell, M. 2008, MNRAS, 389, 585
Fabricius, C., Høg, E., Makarov, V. V., et al. 2002, A&A, 384, 180

Henden, A. A., Levine, S. E., Terrell, D., Smith, T. C., & Welch, D. 2012, Journal of the American Association of Variable Star Observers (JAAVSO), 40, 430
Henden, A. A., Welch, D. L., Terrell, D., & Levine, S. E. 2009, in American Astronomical Society Meeting Abstracts, Vol. 214, American Astronomical Society Meeting Abstracts 214, 407.02
Henry, T. J., Jao, W.-C., Subasavage, J. P., et al. 2006, AJ, 132, 2360
Johnson, J. A. & Apps, K. 2009, ApJ, 699, 933
Johnson, J. A., Gazak, J. Z., Apps, K., et al. 2012, AJ, 143, 111
Kalas, P., Liu, M. C., & Matthews, B. C. 2004, Science, 303, 1990
Koen, C., Kilkenny, D., van Wyk, F., & Marang, F. 2010, MNRAS, 403, 1949
Laing, J. D. 1989, South African Astronomical Observatory Circular, 13, 29
Leggett, S. K. 1992, ApJS, 82, 351
Lépine, S., Hilton, E. J., Mann, A. W., et al. 2013, AJ, 145, 102
Mann, A. W., Brewer, J. M., Gaidos, E., Lépine, S., & Hilton, E. J. 2013a, AJ, 145, 52
Mann, A. W., Gaidos, E., & Ansdell, M. 2013b, ApJ, 779, 188
Neves, V., Bonfils, X., Santos, N. C., et al. 2012, a&a, 538, A25
Neves, V., Bonfils, X., Santos, N. C., et al. 2013, A&A, 551, A36
Newton, E. 2013, in Protostars and Planets VI, Heidelberg, July 15-20, 2013. Poster #1K093, 93
Önehag, A., Heiter, U., Gustafsson, B., et al. 2012, A&A, 542, A33
Perryman, M. A. C., Lindegren, L., Kovalevsky, J., et al. 1997, A&A, 323, L49
Pickles, A. J. 1998, PASP, 110, 863
Press, W. H., Teukolsky, S. A., Vetterling, W. T., & Flannery, B. P. 1992, Numerical recipes in FORTRAN. The art of scientific computing
Rajpurohit, A. S., Reylé, C., Allard, F., et al. 2013a, A&A, 556, A15
Rajpurohit, A. S., Reylé, C., Schultheis, M., & Allard, F. 2013b, in SF2A-2013: Proceedings of the Annual meeting of the French Society of Astronomy and Astrophysics, ed. L. Cambresy, F. Martins, E. Nuss, & A. Palacios, 259–264
Reid, I. N., Hawley, S. L., & Gizis, J. E. 1995, AJ, 110, 1838
Reiners, A., Joshi, N., & Goldman, B. 2012, AJ, 143, 93
Rojas-Ayala, B., Covey, K. R., Muirhead, P. S., & Lloyd, J. P. 2010, ApJ, 720, L113
Rojas-Ayala, B., Covey, K. R., Muirhead, P. S., & Lloyd, J. P. 2012, ApJ, 748, 93
Santos, N. C., Israelian, G., & Mayor, M. 2004, A&A, 415, 1153
Schlaufman, K. C. & Laughlin, G. 2010, A&A, 519, A105+
Skrutskie, M. F., Cutri, R. M., Stiening, R., et al. 2006, AJ, 131, 1163
Sousa, S. G., Santos, N. C., Israelian, G., Mayor, M., & Monteiro, M. J. P. F. G. 2007, A&A, in press
Terrien, R. C., Mahadevan, S., Bender, C. F., et al. 2012, ApJL, 747, L38
Valenti, J. A., Piskunov, N., & Johns-Krull, C. M. 1998, ApJ, 498, 851
van Leeuwen, F. 2007, A&A, 474, 653
Weis, E. W. 1993, AJ, 105, 1962
Weisberg, S. 2005, Applied Linear Regression, Wiley Series in Probability and Statistics (Wiley)
Woolf, V. M. & Wallerstein, G. 2005, MNRAS, 356, 963
Woolf, V. M. & Wallerstein, G. 2006, PASP, 118, 218